Temporal Variation and Vertical Structure of the Marine Atmospheric Mixed Layer over the East China Sea from Mie-Scattering Lidar Data

Temporal Variation and Vertical Structure of the Marine Atmospheric Mixed Layer over the East China Sea from Mie-Scattering Lidar Data

Masatoshi Kuribayashi[1], Toshimasa Ohara[2], and Atsushi Shimizu[2]

[1]*Graduate School of Life and Environmental Sciences*, *University of Tsukuba, Tsukuba, Japan*
[2]*National Institute for Environmental Studies*, *Tsukuba*, *Japan*

Abstract

The marine atmospheric mixed layer (MAML) has an important influence on the diffusion of air pollutants over the East China Sea. We analyzed seasonal and diurnal variations and the vertical structure of the MAML by using continuous Mie-scattering lidar data recorded from March 2008 to February 2010 at Cape Hedo, Okinawa Island, Japan. The height of the MAML showed clear seasonal variation: a summer minimum and a winter maximum, and was significantly correlated with thermal stability (S_t), which we defined as sea surface temperature minus the temperature at the 850 hPa level. The height of the MAML showed minor diurnal variations in summer: a nighttime minimum and a daytime maximum. We detected the entrainment layer between the MAML and the free atmosphere by analysis of the intensity of fluctuations of aerosol concentrations determined from lidar data. Both the intensity of the fluctuations and the thickness of the entrainment zone increased with increasing S_t. The altitude of maximum fluctuation was a little above the top of the MAML.

1. Introduction

Atmospheric pollutants originating in East Asia are transported over long distances to Japan. Ohara et al. (2008) used a chemical transport model and light detection and ranging (lidar) observation data to show that air pollutants are transported over the East China Sea in the mixed layer. The structure of the marine atmospheric mixed layer (MAML) over the East China Sea is an important factor in chemical transport models used to predict the behavior of pollutants in East Asia.

Leduc-Leballeur et al. (2011) used radiosonde data to show that the height of the MAML in the Gulf of Guinea increases with increasing sea surface temperature (*SST*). Sempreviva et al. (2010) used radiosonde and ceilometer data acquired over the Mediterranean to show that the vertical structure of the MAML is dependent on synoptic conditions, such as advection by different air masses.

The Kuroshio Current in the East China Sea flows northeastward along the eastern edge of the continental shelf. The commencement of cold and dry polar continental air advection over the East China Sea during winter strengthens heat flux at the air−sea interface. Consequently, the upward sensible heat flux in winter is higher than in other seasons (Ishii and Kondo 1993). There have been several intensive observation programs over the East China Sea in winter, for example, the Air Mass Transformation Experiment (Agee and Lomax 1978). Shinoda et al. (2009) used radiosonde data and numerical simulations to show the structure of convective circulation in the MAML in summer. However, the behavior of the MAML over the East China Sea through an entire year has not been revealed.

Routine radiosonde soundings at Minami-daito Island provide useful data for year-round observation of the MAML over the East China Sea. However, data are available only at 0830 and 2030 Japan Standard Time (JST), and the vertical resolution of the radiosonde data is too coarse to resolve the fine details of the

MAML structure, such as the entrainment zone at the top of the MAML. On the other hand, lidar data are useful for continuous and detailed measurement of the MAML, including entrainment (e.g., Hageli et al. 2000). Thus, the Mie-scattering lidar equipment at Cape Hedo can provide detailed observations of the temporal variations and vertical structure of the MAML over the East China Sea.

In this study, we estimated the height of the MAML over the East China Sea by using both radiosonde data and lidar data, and statistically compared the results. We then considered the seasonal and diurnal variations of the height of the MAML and their dependency on thermal stability (S_t) based on the continuous lidar data. We also analyzed the vertical structure of the MAML, especially the entrainment zone at the top of the MAML.

2. Data and methodology

2.1 Radiosonde and lidar data

We used radiosonde data from Minami-daito Island (25.83°N, 131.23°E; 17 m elevation) and Mie-scattering lidar data from Cape Hedo (26.87°N, 128.26°E; 60 m elevation) to estimate the height of the MAML for the period from March 2008 to February 2010. Minami-daito Island is about 6 km in diameter and Cape Hedo is at the northern tip of Okinawa Island. The horizontal distance between Minami-daito Island and Cape Hedo is 320 km.

Radiosonde observations are recorded by the Japan Meteorological Agency (JMA) twice daily at 0830 and 2030 JST. The radiosonde data contain observed values at various heights including standard isobaric surfaces. It is noteworthy that the vertical resolution of the data is higher around particular points of the temperature and relative humidity profiles, such as at the top of mixed layer. We used potential temperature θ to estimate the height of the MAML.

Lidar observations recorded at Cape Hedo by the National Institute for Environmental Studies of Japan are made at 15-min intervals. Details of the lidar technique were described by Shimizu et al. (2011). In our study, we used the extinction coefficient of a spherical aerosol at 532 nm, α, with vertical resolution of 30 m, to estimate the height of the MAML.

For our analysis of the vertical structure of the MAML from lidar data, we used backscatter intensity data recorded from the end of December 2008 to the beginning of June 2009. One profile of backscatter intensity, comprising 100 shots, is obtained over a period of 10 sec, and 30 sequential profiles are obtained over a period of 5 min. The continuous 5-min observations are repeated with 10-min breaks between observations. Backscatter intensity data are recorded at 6-m intervals from the ground surface to 3000 m above ground level. Because backscatter intensity is approximately proportional to aerosol concentration, we consider that fluctuations of backscatter intensity around the top of the MAML are associated with the turbulence at the entrainment zone (Boers and Eloranta 1986).

2.2 Estimation of height of MAML

To avoid the influence of land, we analyzed only data from more than 300 m above ground level. Furthermore, we used data recorded only when the speed of wind coming from the sea was greater than 1 m s^{-1} below the 850 hPa level. We defined winds from the sea at Cape Hedo as those approaching the lidar station

from within the arc from south-southwest clockwise to east-southeast. At Minami-daito Island, we considered that all winds were from the sea. We used JMA mesoscale analysis (MANAL) data, which provides upper wind data at the 1000, 975, 950, 925, 900, and 850 hPa levels every 3 h, to screen out winds approaching Cape Hedo from the land. To negate the influence of cloud, we excluded data when the lidar detected clouds below 3000 m altitude.

We defined the height of the MAML determined from radiosonde data, H_θ, as the lowest height at which the vertical gradient of potential temperature, $\Delta\theta/\Delta z$, was greater than or equal to 6 K km^{-1} between two observation levels (Sasano et al. 1982), or as the lowest height at which $\Delta\theta/\Delta z$ was greater than or equal to 2 K km^{-1} for four successive observation levels. We defined the height of the MAML determined from lidar data, H_α, as the lowest height for which α was greater than 5.0×10^{-5} m^{-1} and the vertical gradient, $(\alpha_z - \alpha_{z-\Delta z})/\alpha_z$, was less than -0.08.

3. Results

3.1 Height of MAML from lidar and radiosonde data

Table 1 shows our statistical comparison of H_θ and H_α at 0830 and 2030 JST. There is a significant correlation between H_θ and H_α ($R \geq 0.5$) regardless of time. The means of H_θ and H_α at both 0830 and 2030 JST are consistent, as *MB* (*NMB*) at 0830 JST is -18 m (-2.1%) and *MB* (*NMB*) at 2030 JST is 46 m (5.1%). On the other hand, there are some disagreements between H_θ and H_α, as both *RMSE* and *NME* values are high. We conjecture that the disagreements are caused by one or more of the following: (1) the existence of a floating aerosol layer near the top of MAML over Cape Hedo; (2) the stable layer at the top of the MAML is too small to be detected by radiosonde; (3) the lidar data are provided as 5-min averages, whereas the radiosonde data are instantaneous observations, as discussed by Cooper et al. (1996); and (4) the horizontal distance between Minami-daito Island and Cape Hedo is 320 km, although Stull (1988) mentioned that the height of the MAML varies by only 10% over horizontal distances of 1000 km.

3.2 Temporal variations of height of MAML
a. Seasonal variation

We identified clear seasonal variations of both H_θ and H_α (Fig. 1): both are low in summer and high in winter. The height of the MAML is lowest in July (H_θ, 601 m; H_α, 626 m) and highest in December (H_θ, 1228 m; H_α, 1196 m). The seasonal variation of sensible heat flux from the East China Sea to the atmosphere estimated by Ishii and Kondo (1993) also shows a minimum in summer and a maximum in winter. The seasonal variations of the height of the MAML correspond reasonably well to those of sensible heat flux, though there are small differences. For example, the height of the MAML in February is about 300 m lower than
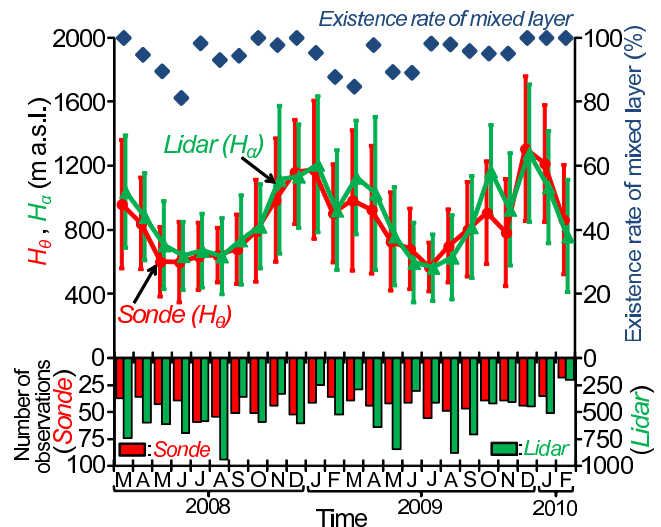

Fig. 1. Seasonal variations of monthly mean height of the MAML estimated by radiosonde (H_θ) and by lidar (H_α) from March 2008 to February 2010. The red line denotes H_θ and the green line denotes H_α, and each error bar shows standard deviation. The red and green bar charts indicate the number of radiosonde and lidar observations, respectively. Existence rate of the MAML is defined in Section 3.2.

that in January, despite the comparable sensible heat flux in January and February. The height of the MAML during the cold season (Nov−Apr) tends to change abruptly (e.g., the difference between November and December in 2009 is 524 m for H_θ and 353 m for H_α). On the other hand, there is little variation of the height of the MAML during June, July, and August, and the error bars in summer are smaller than in other seasons (Fig. 1). Thus, the height of the MAML in summer is less variable than in other seasons.

Figure 2 shows the relationship of daily mean H_α to daily mean thermal stability, S_t (we defined as *SST* minus temperature at 850 hPa altitude), for each season from March 2008 to February 2010. To calculate S_t, we used the *SST* determined daily by the JMA at about 1100 JST near Cape Hedo on the basis of satellite data calibrated with buoy and ship observations (Guan and Kawamura 2004). We neglected the diurnal variation of *SST*, because, unless surface wind speed is less than 2 m s^{-1}, the diurnal range of *SST* is less than 1.5 K (Webster et al. 1996). For the temperature at the 850 hPa level over Cape Hedo, we used data recorded in MANAL every 3 h. Thus, we used up to eight S_t values when calculating the daily mean.

Table 1. Statistical comparison of heights of the MAML determined by radiosonde (H_θ) and by lidar (H_α) at 0830 and 2030 JST.

Time	Mean height		*MB*	*NMB*	*RMSE*	*NME*	*R*	*N*
	H_θ	H_α						
(JST)	(m a.s.l.)	(m a.s.l.)	(m)	(%)	(m)	(%)		(days)
0830	876	858	-18	-2.1	351	29.5	0.58	177
2030	927	973	47	5.1	398	30.8	0.50	122

MB, NMB, RMSE, NME, R, and *N* are mean bias, normalized mean bias, root mean square error, normalized mean error, correlation coefficient, and number of observations, respectively.

$$MB = \sum_1^N (H_{\alpha i} - H_{\theta i})\big/N, \quad NMB = \sum_1^N (H_{\alpha i} - H_{\theta i}) \times 100\big/\sum_1^N (H_{\theta i})$$

$$RMSE = \sqrt{\sum_1^N (H_{\alpha i} - H_{\theta i})^2 \big/ N},$$

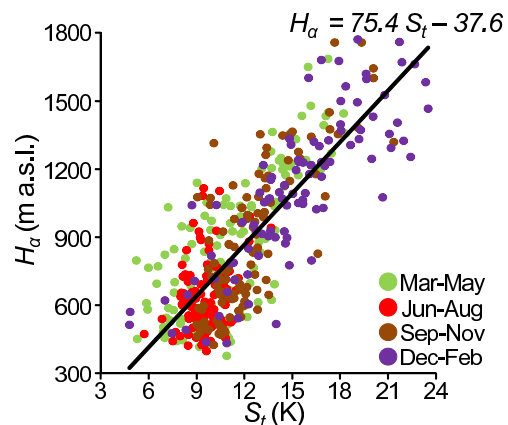$$NME = \sum_1^N |H_{\alpha i} - H_{\theta i}| \times 100\big/\sum_1^N (H_{\theta i})$$

Fig. 2. Scatter plot of daily mean thermal stability (S_t) versus daily mean height of the MAML estimated by lidar (H_α) from March 2008 to February 2010. Data points are color-coded by season. The linear regression line for all data is also shown.

There is a significant correlation ($R = 0.81$, $N = 445$) between daily mean H_α and daily mean S_t. The height of the MAML is associated with S_t. The slope of the regression line indicates that H_α increases approximately 75 m for each 1 K increment of S_t. The correlation coefficients for H_α and S_t are 0.75, 0.27, 0.77, and 0.83 for spring (Mar−May), summer (Jun−Aug), autumn (Sep−Nov), and winter (Dec−Feb), respectively. We suppose that the low correlation coefficient in summer is caused by the relatively constant S_t around 9 K (Fig. 2). The height of the MAML in summer might be affected by the mixing ratio of water vapor rather than by S_t, because the contribution of moisture to buoyant flux is greater than that of heat (Shinoda et al. 2009).

We also investigated whether or not the MAML exists over the East China Sea throughout the year. We defined the existence or non-existence of the MAML as follows: If H_θ was detected at the lowest level used in this study, we considered that thermal conditions were stable and the MAML was absent. In Fig. 1. "Existence rate" represents the percentage of observations in each month for which we determined the MAML to be present. The existence rate was greater than 80% for every month, and the number of radio-sonde observations was about 48 during the warm season (May−Oct) and about 39 during the cold season (Nov−Apr). Therefore, the existence of the MAML over the East China Sea is relatively consistent throughout the year, but it is absent more often in spring and summer than in autumn and winter.

b. Diurnal variation

There have been a few previous studies of diurnal variation of the height of the MAML. For example, Betts et al. (1995) reported a predawn maximum in the North Atlantic (28°N, 24°W) on the basis of 3-hourly sonde data, whereas Johnson et al. (2001) reported an afternoon maximum in the tropical zone of the western Pacific from 6-hourly sonde data. We analyzed the diurnal cycle of the MAML throughout the year by using lidar measurements over the East China Sea (Fig. 3). The difference of the maximum and minimum values of H_α was 28% of daily mean H_α in summer, whereas it was 17−19% in other seasons. Thus, there is a small (about 150 m) diurnal variation of the height of the MAML, especially in summer: a nighttime minimum and a daytime maximum. Johnson et al. (2001) showed similar diurnal variations and explained that the diurnal cycle of the height of the mixed layer was caused by the relatively large (up to 2−3 K) diurnal cycle of *SST*. Figure 3 also shows that the diurnal variation in winter is comparable in amplitude to the variation in summer, while the diurnal cycle in winter is reversal to the cycle in summer: a day-

time minimum and a nighttime maximum. However, the implication is not clear and needs further consideration.

3.3 Fine vertical structure of the MAML from lidar data

For our analysis of vertical structure of the MAML, we defined μ as the mean and σ as the standard deviation of backscatter intensity over 5-min periods (30 data points) for each height (e.g., Supplement 1). The values of μ and σ are approximately proportional to the mean and standard deviation of aerosol concentration, respectively. We analyzed the profiles of μ and σ/μ from December 2008 to June 2009.

To clarify the relationship between the vertical structure of the MAML and S_t, we examined μ and σ/μ profiles for three ranges of S_t: 3−12 K, 12−15 K, and 15−24 K. The individual S_t ranges were selected to provide an approximately even distribution of samples across the entire range. To eliminate the effect of differences of the height of the MAML, we normalized the heights of the μ and σ/μ profiles by dividing them by H_α, thus producing dimensionless profiles (Figs. 4a and 4b). We then calculated the average value of μ (Fig. 4a) and the median value of σ/μ (Fig. 4b) for each dimensionless height for each S_t range. The profiles of averaged μ in Fig. 4a were normalized by the value at the top of the MAML (dimensionless height = 1).

The three profiles of average μ within the MAML are similarly uniform (Fig. 4a) and decrease above H_α, indicating that aerosols are well mixed below H_α owing to convection, regardless of S_t. In general, the aerosol concentrations are high in the mixed layer and low in the free atmosphere, and there is a transition zone around the top of the mixed layer in which the aerosol concentrations decrease gradually. The median of σ/μ reaches a maximum around H_α (Fig. 4b), reflecting entrainment at the transition zone. Furthermore, if the normalized entrainment thickness is defined as the range over which the median of σ/μ is greater than 0.05, the dimensionless thicknesses of the entrainment layers are 0.25 for S_t of 3−12 K, 0.26 for S_t of 12−15 K, and 0.29 for S_t of 15−24 K. Thus, we consider that the entrainment thickness amounts to about 25−30% of the height of the MAML. Stull (1988) summarized that the average of entrainment thickness is about 40% of the height of the mixed layer based on some researches by lidar measurements and laboratory experiments. Hence the entrainment thickness over East China Sea estimated by this study tends to be thinner than the previous results. However, it is not evident whether the difference is significant because the entrainment thickness depends on the
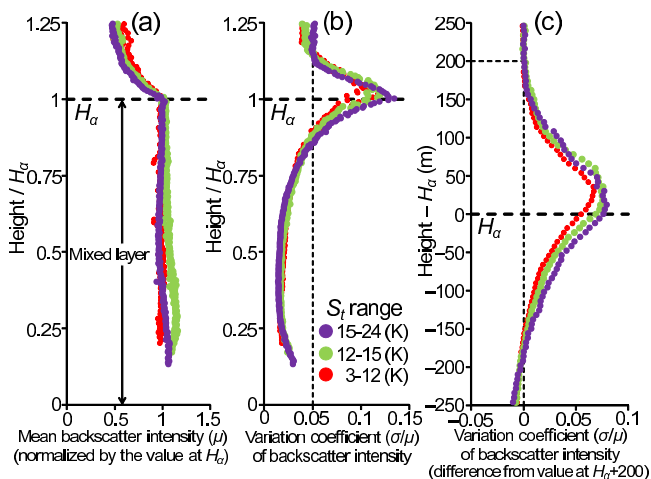
Fig. 4. (a) Dimensionless profiles of the average of the mean backscatter intensity (μ) over 5-min periods for three ranges of thermal stability (S_t) from December 2008 to June 2009. Backscatter intensity was normalized by the value at the top of the MAML. (b) Dimensionless profiles of the median of the coefficient of variation (σ/μ) for each S_t range. (c) Profiles of the median of σ/μ for each S_t range. The value of σ/μ at $H_\alpha + 200$ was subtracted from the value at each data point to negate the effect of signal noise in lidar data (see Section 3.3 for explanation).
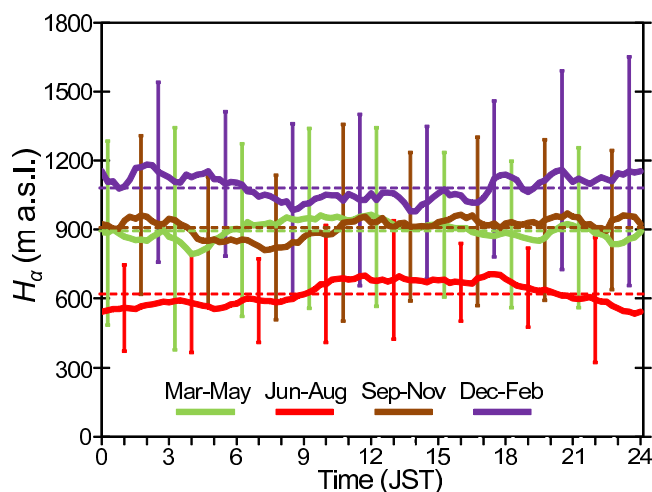

Fig. 3. Seasonal diurnal variations of the height of the MAML estimated from lidar data from March 2008 to February 2010. The green, red, brown, and violet lines indicate spring, summer, autumn, and winter, respectively. Dashed lines and error bars indicate the seasonal means and the standard deviation, respectively.

estimated methods and the definitions.

Figure 4c demonstrates the dependency of the median of σ/μ profiles on S_t around the entrainment zone. To eliminate noise in the lidar data, we calculated the median of σ/μ for each height (6-m intervals) for each S_t range, and subtracted the value of σ/μ at H_a + 200 m from the value at each data point. Noise influences the value of σ for higher altitudes of the MAML, because the noise level is proportional to the square of elevation above the lidar equipment (see Supplement 1). We set the reference level at H_a + 200 m because the vertical profile of the median of σ/μ at H_a + 200 m is nearly constant for each range of S_t. The height of the σ/μ peak is 12−36 m higher than H_a for every S_t range. This result is similar to that of Lammert and Bosenberg (2006), who showed that the height of the mixed layer determined on the basis of aerosol variance is a little higher than that determined on the basis of aerosol gradient. Further, we suggest that the higher the S_t range, the greater the maximum of the median of σ/μ (Fig. 4c), which indicates that entrainment intensity is dependent on S_t. If we define the thickness of the entrainment zone as the range of heights over which the median of σ/μ is greater than zero in Fig. 4c, the thicknesses are 336 m for S_t of 3−12 K, 366 m for S_t of 12−15 K, and 378 m for S_t of 15−24 K. Therefore, we also suggest that the higher the S_t range, the greater the thickness of the entrainment zone.

4. Conclusions

The 30-m resolution lidar from Cape Hedo provides useful data for analysis of seasonal and diurnal variations and of the vertical structure of the MAML over the East China Sea. We estimated the height of the MAML from the gradient of the extinction coefficient of a spherical aerosol measured for 5 min by a 532 nm laser every 15 min from March 2008 to February 2010. We also investigated the vertical structure of the MAML and the thickness of the entrainment zone by using high-resolution lidar backscatter intensity data, for which vertical resolution was 6 m and time resolution was 10 sec, from the end of December 2008 to the beginning of June 2009.

The existence of the MAML over the East China Sea was relatively consistent throughout the year. The correlation coefficients between the heights of the MAML determined from lidar data and from radiosonde data were greater than 0.5 at both 0830 and 2030 JST, and the monthly means and seasonal variations determined by both methods were consistent. We found that the height of the MAML had a clear seasonal variation (low in summer and high in winter), which reflects the seasonal variation of S_t. Our analysis showed that the height of the MAML increased by about 75 m for each 1 K increase of S_t. The height of the MAML had a small (about 150 m) diurnal variation in summer: a nighttime minimum and a daytime maximum. The difference of the maximum and minimum of H_a was 28% of daily mean H_a in summer.

The vertical structure of the MAML over the East China Sea is similar to the vertical structure of the mixed layer observed in other studies over land. We found that the vertical profile of aerosol concentrations within the MAML is nearly uniform and independent of S_t. We found that the entrainment zone determined from lidar data amounted to 25−30% of the height of the MAML. The height of the maximum fluctuation of aerosol concentrations was 12−36 m higher than the top of the MAML for the full range of S_t we considered. We suggest that both the intensity of these fluctuations and the thickness of the entrainment zone increase with increasing S_t.

Acknowledgements

Supplement

An example of our analysis of the vertical structure of the MAML from backscatter intensity data is shown in Supplement 1.

References

Agee, E. M., and F. E. Lomax, 1978: Structure of the mixed layer and inversion layer associated with patterns of mesoscale cellular convection during AMTEX 75. *J. Atmos. Sci.*, **35**, 2281−2301.

Betts, A. K., C. S. Bretherton, and E. Klinker, 1995: Relation between mean boundary-layer structure and cloudiness at the R/V *Valdivia* during ASTEX. *J. Atmos. Sci.*, **52**, 2752−2762.

Boers, R., and E. W. Eloranta, 1986: Lidar measurements of the atmospheric entrainment zone and the potential temperature jump across the top of the mixed layer. *Boundary-Layer Meteor.*, **34**, 357−375.

Cohn, S. A., and W. M. Angevine, 2000: Boundary layer height and entrainment zone thickness measured by lidars and wind-profiling radars. *J. Appl. Meteor.*, **39**, 1233−1247.

Cooper, D. I., W. E. Eichinger, S. Barr, W. Cottingame, M. V. Hynes, C. F. Keller, C. F. Lebeda, and D. A. Poling, 1996: High-resolution properties of the equatorial Pacific marine atmospheric boundary layer from lidar and radiosonde observations. *J. Atmos. Sci.*, **53**, 2054−2075.

Guan, L., and H. Kawamura, 2004: Merging satellite infrared and microwave SSTs: Methodology and evaluation of the new SST. *J. Oceanogr.*, **60**, 905−912.

Hageli, P., D. G. Steyn, and K. B. Strawbridge, 2000: Spatial and temporal variability of mixed-layer depth and entrainment zone thickness. *Boundary-Layer Meteor.*, **97**, 47−71.

Ishii, T., and J. Kondo, 1993: The seasonal variation of the oceanic heat transport in the East China Sea, Yellow Sea and Sea of Pohai. *Tenki*, **40**, 895−906, (in Japanese).

Johnson, R. H., P. E. Ciesielski, and J. A. Cotturone, 2001: Multiscale variability of the atmospheric mixed layer over the Western Pacific warm pool. *J. Atmos. Sci.*, **58**, 2729−2750.

Lammert, A., and J. Bosenberg, 2006: Determination of the convective boundary-layer height with laser remote sensing. *Boundary-Layer Meteor.*, **119**, 159−170.

Leduc-Leballeur, M., L. Eymard, and G. de Coetlogon, 2011: Observation of the marine atmospheric boundary layer in the Gulf of Guinea during the 2006 boreal spring. *Quart. J. Roy Meteor. Soc.*, **137**, 992−1003.

Ohara, T., I. Uno, J. Kurokawa, M. Hayasaki, and A. Shimizu, 2008: Episodic pollution of photochemical ozone during 8−9 May 2007 over Japan −Overview−. *J. Japan Soc. Atmos. Environ.*, **43**, 198−208, (in Japanese).

Sasano, Y., A. Shigematsu, H. Shimizu, N. Takeuchi, and M. Okuda, 1982: On the relationship between the aerosol layer height and the mixed layer height determined by laser radar and low-level radiosonde observations. *J. Meteor. Soc. Japan*, **60**, 889−895.

Sempreviva, A. M., M. E. Schiano, S. Pensieri, A. Semedo, R. Tome, R. Bozzano, M. Borghini, F. Grasso, L. L. Soerensen, J. Teixeira, and C. Transerici, 2010: Observed development of the vertical structure of the marine boundary layer during the LASIE experiment in the Ligurian Sea. *Ann. Geophys.*, **28**, 17−25.

Shimizu, A., N. Sugimoto, I. Matsui, I. Mori, M. Nishikawa, and M. Kido, 2011: Relationship between lidar-derived dust extinction coefficients and mass concentrations in Japan. *SOLA*, **7A**, 1−4.

Shinoda, T., A. Higuchi, K. Tsuboki, T. Hiyama, H. Tanaka, S. Endo, H. Minda, H. Uyeda, and K. Nakamura, 2009: Structure of convective circulation in the atmospheric boundary layer over the Northwestern Pacific Ocean under a subtropical high. *J. Meteor. Soc. Japan*, **87**, 979−996.

Stull, R. B., 1988: *An Introduction to Boundary-Layer Meteorology*. Kluwer Academic Publishers, 666 pp.

Webster, P. J., C. A. Clayson, and J. A. Curry, 1996: Clouds, radiation, and the diurnal cycle of sea surface temperature in the Tropical Western Pacific. *J. Climate*, **9**, 1712−1730.